Journal of Power Sources 193 (2009) 617–624

Contents lists available at ScienceDirect

Journal of Power Sources

journal homepage: www.elsevier.com/locate/jpowsour

Effect of various coal contaminants on the performance of solid oxide fuel cells: Part II. ppm and sub-ppm level testing

JianEr Bao*, Gopala N. Krishnan, Palitha Jayaweera, Kai-Hung Lau, Angel Sanjurjo

SRI International, 333 Ravenswood Ave., Menlo Park, CA 94025, USA

ARTICLE INFO

Article history:
Received 5 February 2009
Received in revised form 14 April 2009
Accepted 15 April 2009
Available online 3 May 2009

Keywords:
Solid oxide fuel cell
Fuel contaminants
Performance degradation
Poisoning effect
Thermochemical property

ABSTRACT

The poisoning effects of various trace contaminants in the coal-derived syngas stream at ppm and sub-ppm level on the performance of Ni-YSZ/YSZ/LSM solid oxide fuel cells were studied at extended duration. The thermochemical nature of impurities such as $PH_3(g)$ and $CH_3Cl(g)$ in presence and absence of water steam was analyzed by a high temperature mass spectrometer. Only less than half of $PH_3(g)$ is hydrolyzed, and $CH_3Cl(g)$ also co-exist with $HCl(g)$. After a certain duration of exposure, 1 ppm $AsH_3(g)$, 0.5 ppm $PH_3(g)$, and 2.5 ppm $CH_3Cl(g)$ all caused some degree of degradation to the power density at 750 °C. Whereas 1 ppm of $H_2S(g)$ resulted in immediate performance loss. The mechanisms of degradation are mainly divided into two categories: surface adsorption effect (for S and Cl) and bulk reaction effect (for As and P). The controversies regarding the poisoning effect and mechanism of S are also discussed with the aid of thermodynamic equilibrium composition calculation.

1. Introduction

Currently, the integrated coal gasification-fuel cell (IGFC) technology that produces electricity from the cleaned up gas stream of a coal gasifier is one of the pursued clean energy technologies by the U.S. Department of Energy's Solid State Energy Conversion Alliance (SECA) program. However, previous research has shown that many trace impurities would form volatile species under the gasification and warm/hot or cold gas cleanup conditions, and end in the coal-derived fuel gas stream to reach the solid oxide fuel cell (SOFC) [1]. The best data available for the potential trace impurities and their concentration level are from a process that is being used for the production of methanol from coal-derived gas at the Eastman Chemical Company's chemicals from a coal complex at Kingsport, TN. It indicated that the following contaminants may be present after the coal gas has undergone Rectisol (cold) cleanup [2]: AsH_3 = 0.15–0.58 ppm; CH_3Cl = 2 ppm; CH_3SCN = 2.1 ppm, $Fe(CO)_5$ = 0.05–5 ppm; HCl = <1 ppm; $Ni(CO)_5$ = 0.001–0.025 ppm; PH_3 = 1.9 ppm; Sb = 0.025 ppm; and Zn = 9 ppm. These trace level impurities may interact with the anode electrocatalyst and cause the degradation of the cell performance in a short or long duration.

In a previously published manuscript (Part I [3]), accelerated testing was carried out using anode-supported Ni-YSZ/YSZ/LSM (YSZ stands for yttria-stabilized zirconia, and LSM stands for lanthanum strontium manganese oxide) cells to inspect whether degradation occurred at a relatively high concentration level of each impurity within a short period of exposure time (~100 h). The results showed that As and P species could most likely cause considerable cell performance degradation at 800 °C and below by forming compounds with the anode catalyst or the current collector; while the presence of chlorine species and Cd(g) affected the cell performance only at temperatures above 800 °C; and other volatile impurities such as Hg(g), Zn(g), and SbO(g) only resulted in less than 1% degradation over the time tested. In the present work, extended tests were carried out to ascertain whether these impurities, at typical concentration levels in the coal-derived syngas stream, would cause long-term degradation to the cell performance.

Thermochemical forms of some impurity species in the fuel gas stream after warm/cold gas cleanup technology and at the SOFC operating environment, as well as possible reactions with the anode catalyst have been discussed by a few researchers using thermodynamic calculations [1,4]. Thermochemical equilibrium analysis helps to better understand the possible interactions between the impurity and the anode. However, no experimental manifestations are currently available. In this work, high temperature mass spectrometry was used to detect the thermochemical forms of some of these impurities at the operating temperature range of the SOFCs, along with some thermodynamic calculations and discussions of possible reactions with the anode catalyst.

* Corresponding author.
E-mail address: valeriebao@gmail.com (J. Bao).

0378-7753/$ – see front matter © 2009 Elsevier B.V. All rights reserved.
doi:10.1016/j.jpowsour.2009.04.035

2. Experimental

The cell preparation method, experimental setup, electrochemical measurement, and after experiment characterization have been described in a previous paper [3], and will only be briefly mentioned here. The SOFCs used are anode-supported type as Ni-YSZ/YSZ/LSM, with the thickness of each layer being 5–10 μm, 4–6 μm, and 30–60 μm. The anode support layer (YSZ) is 465–555 μm thick. A nickel mesh bonded to the anode by nickel paste is used as the anode current collector, and gold wires bonded to the cathode by platinum paste are used as the cathode current collector. In this work, the trace amounts of impurities were introduced by passing a carrier gas through G-Cal permeation devices from VICI Metronics. Each permeation device has a calibrated, known permeation rate, and the concentration, C, of the trace impurity gas in ppm level, can be calculated from the following equation:

$$C = \frac{K\ P}{F} \quad (1)$$

where K is a constant related with the volume of gas per each nanogram of that gas molecule at the standard condition in ml/ng, P is the gas permeation rate at ambient temperature in ng/min, and F is the carrier gas flow rate in ml/min. The total flow rate for the coal-derived syngas stream is approximately 100 ml min^{-1}, with the composition of the syngas being: 30% CO, 30.6% H_2, 11.8% CO_2, and 27.6% H_2O.

Thermochemical properties of PH_3(g) and CH_3Cl(g) gas in presence and absence of water vapor were measured by a high temperature mass spectrometer using a 30.5 cm radius, single focusing, magnetic deflection instrument described in literature [5–7]. This system has been reliably used to measure high temperature thermodynamic properties of many inorganic chemicals for over 30 years. The spectrometer is composed of a heated molecular effusion-beam vapor source, an electron impact ion source, and a magnetic mass analyzer, as illustrated in Fig. 1.

The effusion-beam vapor source has the Knudsen cell configuration which is a direct molecular beam sampling system: chemistry of the species in the cell is frozen in the collision free molecular effusion beam which has a line-of-sight path from the Knudsen cell orifice (1.0 mm diameter) to the ion source without encountering any surfaces. The ionized particles are then accelerated and analyzed by the magnetic mass analyzer. The intensity of each ion signal is measured at 3 eV above its appearance potential to eliminate overlapping contributions from ions formed by fragmentation processes. Ion intensities are then converted to partial pressures, P_i, from the relation

$$P_i = \frac{kI_i^+T}{\sigma_i} \quad (2)$$

where I^+ is the ion intensity, T is the temperature in Kelvin, σ_i is the relative ionization cross section for each specie i, and k is an instrument sensitivity constant evaluated using a high-purity sample such as Au or Sn as a vapor pressure standard. The derived partial pressures are estimated to be accurate within a factor of two, based on considerable past experience. The lower pressure detection limit for most observed species is on the order of 5×10^{-11} atm.

The reactant gas PH_3 was admitted to the base inlet of the quartz effusion Knudsen cell through a precision molecular leak valve from an external Ar carrier system. Trace levels of impurity gas was generated by passing Ar at 2–3 ml min^{-1} rate through a PH_3 permeation device with a known permeation rate. While trace levels of CH_3Cl gas was introduced into the Knudsen cell from a certified gas mixture cylinder. Deionized H_2O was frozen and then held under vacuum to remove dissolved gases and it was added separately to the gas mixture from an external metering system with a precision needle valve. The cell was packed with quartz chips to insure temperature equilibration of the gas mixture when the gas was heated to study the thermal decomposition behavior.

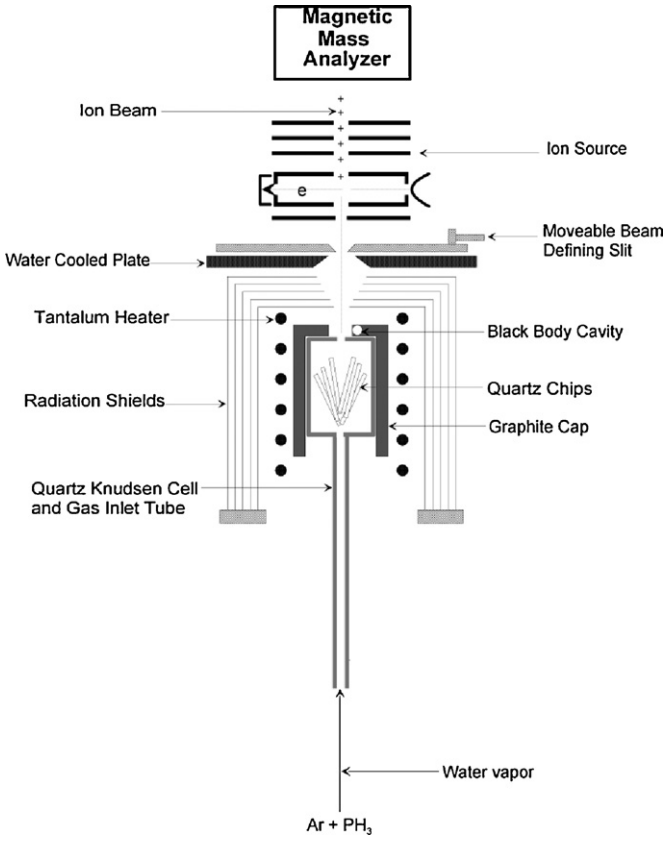

Fig. 1. A schematic illustration of the layout of the high temperature mass spectrometer and the effusion source inside the spectrometer chamber.

STANJAN program, developed at Stanford University for calculating chemical equilibria in complex systems, was used for the thermochemical calculations in this work. The thermodynamics data for the H–P–O species are selected from the compilation of Gurvich et al. [8], and the new values for HPO, HPO_2 and HPO_3 are from our previous study [9]. A new STANJAN-compatible database for species in the H-P-O system for equilibrium calculations are being developed in this lab. HSC chemistry® program from Outokumpu was also used for phase stability and equilibrium compositions study.

3. Results and discussions

3.1. Thermal decomposition behavior of PH_3(g)

The mass spectra of Ar and PH_3 gas mixture in absence and presence of water are analyzed at ambient temperature of 293 K (20 °C) and at cell temperature of 995 K (722 °C). The measured and also calculated equilibrium partial pressures for each species detected after thermal decomposition of PH_3 in absence and presence of water are listed in Tables 1 and 2, respectively. In Table 1, thermochemical calculations show that in absence of water, PH_3 will decompose to P_2 and P_4 even at ambient temperature. However, at 995 K, the measured partial pressures for P_2 and P_4 are still very low, and PH_3 is the dominating chemical form of phosphor containing specie. This clearly indicates that PH_3 does not decompose easily to reach the thermal equilibrium condition at the SOFC operating temperature in absence of water vapor.

Table 1
Comparison of the measured and calculated partial pressures of the observed vapor species for Ar + PH_3 mixture.

Species	Partial pressures (atm)			
	293 K		995 K	
	Measured	Calculated	Measured	Calculated
Ar	1.16×10^{-4}	1.00×10^{-4}	3.96×10^{-4}	5.00×10^{-4}
PH_3	6.36×10^{-9}	1.13×10^{-19}	2.36×10^{-8}	8.63×10^{-19}
P_2		1.46×10^{-21}	5.57×10^{-11}	1.00×10^{-8}
P_4		1.00×10^{-9}	2.13×10^{-9}	1.07×10^{-12}
H_2		6.00×10^{-9}		3.00×10^{-8}

Table 2 shows that in presence of water vapor at 995 K, HPO_2 and HPO_3 species are formed by the reaction of PH_3 with steam:

$$PH_3(g) + 2H_2O(g) = HPO_2(g) + 3H_2(g) \quad (3)$$

$$PH_3(g) + 3H_2O(g) = HPO_3(g) + 4H_2(g) \quad (4)$$

These hydrolyzed phosphorous species may react with the YSZ phase of the anode forming yttrium or zirconium phosphate compounds or may react with Ni electrocatalyst forming nickel phosphate [10]. The former could decrease the transport of oxygen ion through the YSZ network, and the latter could deteriorate the catalytic activity of Ni.

The results shown in Table 2 also indicate that the decomposition of $PH_3(g)$ is limited kinetically even at 995 K. In presence of highly excess steam ($H_2O/PH_3 \sim 6000$), the observed fraction of the $HPO_3(g)$ vapor is significantly less than that predicted by the equilibrium calculations. Therefore, some fraction of unconverted PH_3 may reach the anode to react with the Ni phase as well forming nickel phosphides.

3.2. Thermal decomposition behavior of $CH_3Cl(g)$

In the previous paper, it was shown that $CH_3Cl(g)$ degraded the power density of the SOFC more than HCl(g) at the same concentration level. Thermodynamic equilibrium calculations predicted that under anode gas conditions, $CH_3Cl(g)$ will be fully converted to HCl(g). To determine experimentally the fate of the $CH_3Cl(g)$ under the SOFC operating conditions, 500 ppm level $CH_3Cl(g)$ was introduced to the Knudsen cell along with H_2 and H_2O. Tables 3 and 4 show the partial pressures of detected species when $CH_3Cl(g)$ and H_2 are in absence and presence of H_2O vapor, respectively.

Table 3 shows that at 1023 K with the absence of steam, $CH_3Cl(g)$ decomposed, but the amount of HCl(g) converted is much less than that predicted by thermodynamic equilibrium calculations, and $CH_3Cl(g)$ is still the main specie detected. After the addition of steam, Table 4 shows that the extent of conversion increased significantly, though there still existed some portion of $CH_3Cl(g)$.

Overall, the presence of steam enhances the hydrolyzation and decomposition of $PH_3(g)$ and $CH_3Cl(g)$, respectively. However, the extent of conversion is less than that predicted by equilibrium calculations, in any case. When considering the interactions between these impurities and the anode catalyst, all the species need to be included.

Table 2
Comparison of the measured and calculated partial pressures of the observed vapor species for Ar + PH_3 + H_2O mixture at 995 K.

Species	Partial pressures (atm)		
	Measured (without H_2O)	Measured (with H_2O)	Calculated (with H_2O)
Ar	3.96×10^{-4}	3.96×10^{-4}	4.17×10^{-4}
PH_3	2.36×10^{-8}	1.26×10^{-8}	1.51×10^{-28}
H_2O		7.60×10^{-5}	8.33×10^{-5}
HPO			1.22×10^{-15}
HPO_2		1.70×10^{-9}	1.20×10^{-9}
HPO_3		7.20×10^{-9}	1.54×10^{-8}
H_2			6.55×10^{-8}
O			1.27×10^{-16}
OH			4.30×10^{-12}
O_2			8.97×10^{-14}
PO			1.12×10^{-14}
PO_2			3.20×10^{-12}
P_2	5.57×10^{-11}		2.95×10^{-27}
P_4	2.13×10^{-9}		9.29×10^{-51}

Table 3
Comparison of the measured and calculated partial pressures of the observed vapor species for H_2 + 500 ppm CH_3Cl mixture.

Species	Partial pressures (atm)			
	293 K		1023 K	
	Measured	Calculated	Measured	Calculated
CH_3Cl	7.59×10^{-8}	1.91×10^{-26}	2.12×10^{-7}	9.85×10^{-34}
H_2	7.61×10^{-5}	3.00×10^{-4}	2.56×10^{-4}	3.00×10^{-4}
$P(CH_3Cl)/P(H_2)$	9.98×10^{-4}		8.29×10^{-4}	
CH_4		1.50×10^{-7}	3.49×10^{-8}	6.97×10^{-9}
HCl		1.50×10^{-7}	8.43×10^{-8}	1.50×10^{-7}

3.3. Effect of sub-ppm level Hg(g)

Tests with sub-ppm levels of Hg vapor (~180 ppb) were performed at RTI International, Research Triangle Park, NC, at constant temperatures of 750 °C, 800 °C, and 850 °C. Initially, the cells were kept at the operating temperature in a contaminant-free simulated coal-derived gas stream for more than 50 h to obtain steady state conditions at a constant current load of 1 A (222 mA cm^{-2}). Previously, we have shown that the cells were stable for 400 h in absence of any contaminants. After this initial break-in period, the contaminant was introduced and the change in the power density as a function of time was recorded. Fig. 2 illustrates the time evolution of the cell power density at a series of temperatures and under ~180 ppb Hg(g) exposure. The *Y*-axis of the data at 850 °C is offset by 20 mW cm^{-2} with that of the others in order to show the tendency clearly. Note, the same cell was used for the exposure at three different temperatures since there was no degradation at 750 °C and later at 800 °C within the test period (from the previous accelerated tests at phase I of this project [3], it seems that for metallic contaminants, the degradation effect is more severe at higher temperatures). However, it must be pointed out that this may lead to some misinterpretation of the data.

From the figure, it is seen that the cell performance experienced no decline during the exposure at 750 °C and 800 °C for roughly 120 h each, and that the power density even improved over the time. The *i–v* curve before and after exposure at each temperature (not shown) showed slight performance increase as well. The cause

Table 4
Comparison of the measured and calculated partial pressures of the observed vapor species for H_2 + 500 ppm CH_3Cl + H_2O mixture at 1023 K.

Species	Partial pressure (atm)		
	Measured (without H_2O)	Measured (added H_2O)	Calculated[a]
CH_3Cl	2.12×10^{-7}	9.54×10^{-8}	3.05×10^{-17}
H_2	2.56×10^{-4}	2.59×10^{-4}	2.18×10^{-4}
$P(CH_3Cl)/P(H_2)$	8.29×10^{-4}	3.65×10^{-4}	
CH_4	3.49×10^{-8}	9.89×10^{-8}	3.69×10^{-9}
HCl	8.43×10^{-8}	1.57×10^{-7}	6.82×10^{-8}
CO		1.84×10^{-7}	8.18×10^{-5}
CO_2			2.43×10^{-9}
H_2O		3.91×10^{-5}	4.97×10^{-9}

[a] Calculation was based on $C/H_2/H_2O/CH_3Cl = 1/1/0.6/500$ ppm mole ratio in the graphite Knudsen cell and at 3.0×10^{-4} atm total pressure.

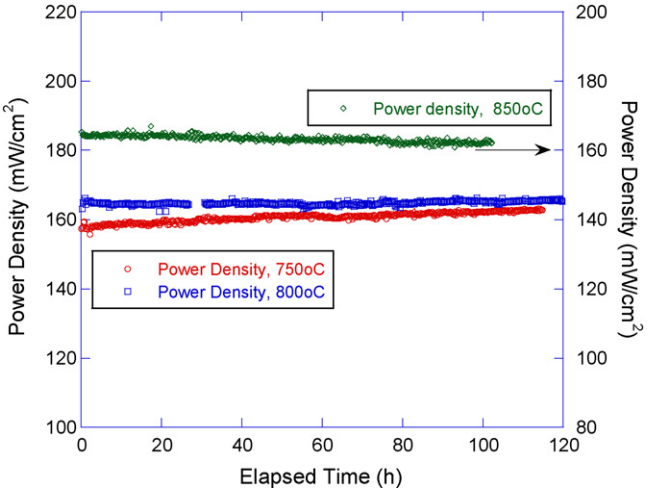

Fig. 2. Time evolution of the cell performance during the exposure to 180 ppb Hg(g) at a series of temperatures: 750 °C, 800 °C, and 850 °C.

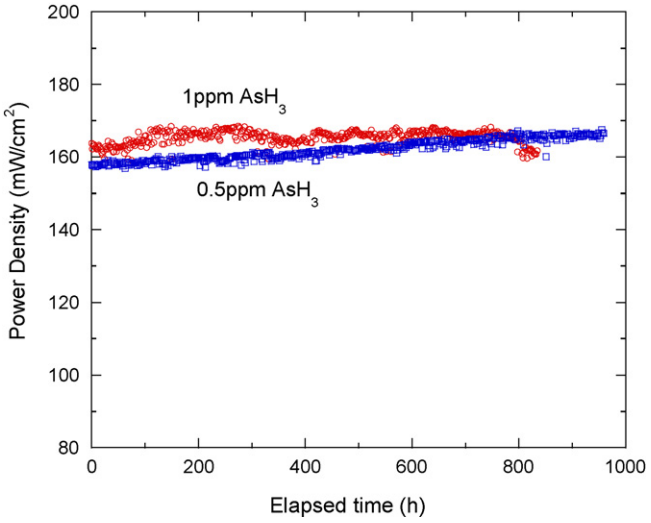

Fig. 3. SOFC performance variation during the exposure to 0.5 ppm and 1 ppm AsH_3(g) at 750 °C.

for the improvement may not be the effect of the Hg(g), and might be that the cell was not fully conditioned to its optimum performance when the contaminant was introduced. At 850 °C, however, a very slight decline is observed at the beginning of the test, and then the cell power density remained steady. The slight decline may be due to the further sintering of the Ni catalyst at higher temperatures, and not attributed to the effect of 180 ppb Hg(g). Therefore, at such low level, mercury contaminant is most likely not to cause any degradation to the SOFC performance.

3.4. *Effect of sub-ppm level AsH_3(g)*

Two concentration levels of arsine were tested at 750 °C: one at 0.5 ppm level using a permeation device from VICI Metronics (permeation rate: 154 ng min^{-1}, in approximately 100 ml min^{-1} fuel stream. The K factor for AsH_3 is 0.313), and the other one at 1 ppm using a gas cylinder containing a calibrated quantity of arsine gas. The cells were maintained at the operating temperature in a contaminant-free simulated coal-derived gas stream (100 ml min^{-1}) for more than 200 h to obtain steady state conditions at a current load of 1 A (equivalent to 0.222 A cm^{-2}). The contaminants were introduced after this initial break-in period, and the cell performance during the exposure is shown in Fig. 3 as a function of time. As can be seen in the figure, no degradation occurred to the cell exposed to 0.5 ppm AsH_3 at 750 °C over the 1000 h tested, whereas the cell exposed to 1 ppm AsH_3 showed clear degradation after 700 h and the power density dropped by about 6 mW cm^{-2} (~3.6%) within 120 h (3% per 100 h).

Arsenic is present in the coal-derived syngas in the form of AsH_3(g) in the reducing environment of gasification and in the form of As_4(g) vapor after warm gas cleanup [11,12]. Thermodynamically, both these trace arsenic species have the potential to react with Ni and form nickel arsenides. Fig. 4 shows the equilibrium compositions of the arsenic containing species calculated by HSC Chemistry® software when Ni anode is exposed to the simulated coal-derived syngas with trace amount of arsenic species (initial composition: H_2 30 mol%, CO 30 mol%, CO_2 12 mol%, and H_2O 28 mol%). From the figure, it can be seen that over 99% of As could be taken up by the Ni catalyst and convert Ni to nickel arsenides with NiAs being the main compound at low AsH_3(g) concentration levels and Ni_5As_2 gradually increasing and surpassing NiAs at 15 ppm AsH_3(g). The figure also shows that nickel arsenides form at sub-ppm arsenic level. Below 2 ppm, the amount of Ni_5As_2 is over 10 times less than that of NiAs, which is probably the reason that XRD analysis for the cell exposed to 1 ppm level and below AsH_3(g) could only find NiAs compound [11]. The formation of NiAs could change the structure and morphology of the anode, and break down the electron transport network. Consequently, the cell performance degrades. The formation of Ni_5As_2 converts more Ni atoms per each As atom, and may cause more severe degradation than NiAs. That probably explains that in our previous accelerated test with 10 ppm AsH_3(g), immediate cell performance degradation was seen. SEM analysis showed that arsenides were only found at the anode surface, which indicated that the kinetics of nickel arsenides formation is fast, and that almost all the arsenic species had reacted with the first several layers of the nickel catalyst. However, at sub-ppm level exposure, the accumulation of the nickel arsenides would take quite a long time for the effect to be clearly seen.

The effect of AsH_3(g) to the performance of SOFCs has been summarized by Cayan et al. [12], including our previous accelerated test with 10 ppm AsH_3. Except that at 10 ppm level, the cell performance showed over 10% degradation within 100 h at 750 °C, and the cell failed at 800 °C due to the nickel contact forming

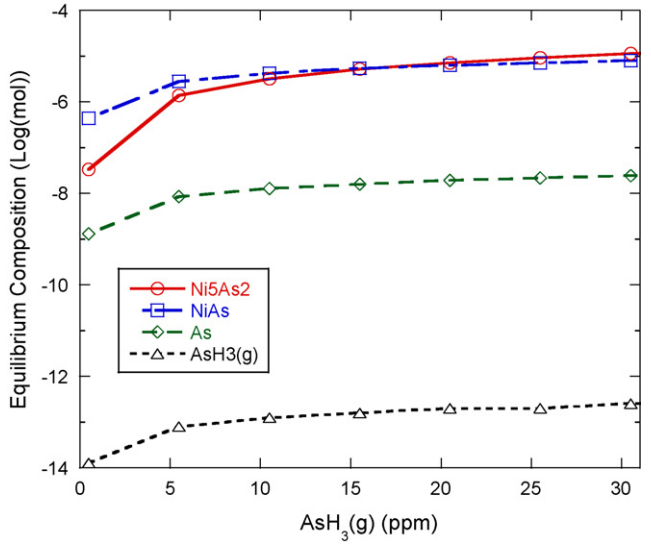

Fig. 4. Equilibrium compositions of the arsenic containing species when the Ni anode is in contact with As contaminated coal-derived syngas. The calculation is based on the initial composition of the simulated syngas.

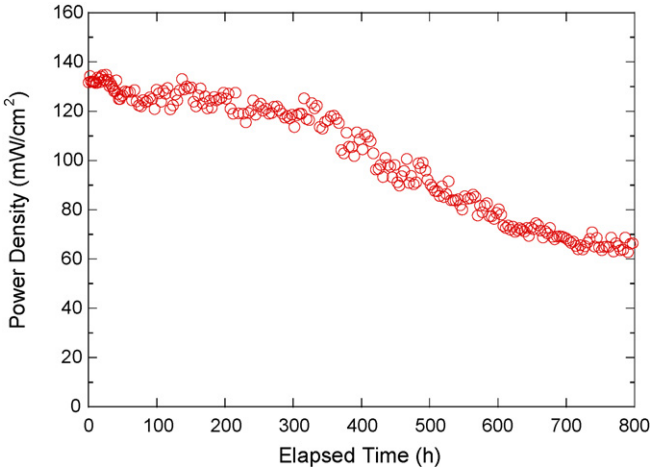

Fig. 5. SOFC performance variation during the exposure to 0.5 ppm $PH_3(g)$ at 750 °C.

arsenides, exposure at 1 ppm level and less all showed only a slight degradation over extended testing: mostly less than 4% over 800 h (<0.5% per 100 h).

3.5. Effect of sub-ppm level $PH_3(g)$

As has been discussed in Section 3.1, the thermochemical nature of phosphorous compounds is complicated in the SOFC operating system. Though thermodynamically, $PH_3(g)$ is expected to be hydrolyzed, kinetically, the conversion is less than half complete. Therefore, $PH_3(g)$ co-exists with $HPO_2(g)$ and $HPO_3(g)$ with $PH_3(g)$ being the main specie. Thermodynamically, the formation of phosphide and phosphate are both favorable under the SOFC operating conditions.

In the test, 0.5 ppm $PH_3(g)$ was introduced by passing a carrier gas (H_2) through a permeation device which releases $PH_3(g)$ at a rate of 178 ng/min (K factor for $PH_3(g)$ is 0.719), while the total coal-derived syngas flow rate was 100 ml min^{-1}. The cell performance at 750 °C after the introduction of sub-ppm level $PH_3(g)$ is shown in Fig. 5. The power density first remained stable for about 30 h, then a slow decline was observed (drop by about 5%), while significant degradation occurred after 300 h and the power density dropped from about 120–60 mW cm^{-2} within 500 h (~0.12 mW/(cm^2 h)).

During the previous accelerated tests [3], it was shown that 35 ppm of phosphorous containing species caused immediate degradation (~10 mW cm^{-2}) followed by a very slow degradation at 750 °C; whereas at 800 °C, a high degradation rate (0.18 mW/(cm^2 h)) was observed. Cayan et al. [12] summarized the effect of phosphorous species to the SOFC performance with the exposure level from 2 ppm to 20 ppm. Only two short-period exposure at 750 °C with 2 ppm and 5 ppm of $PH_3(g)$ [11] are available for direct comparison with our current work. No degradation occurred during the approximately 120 h exposure to 5 ppm $PH_3(g)$, and only very slight degradation was observed with 2 ppm $PH_3(g)$ within ~120 h test. At 800 °C, significant degradation occurred after ~200 h's exposure to 2 ppm $PH_3(g)$, and the power density dropped by 40% after 500 h [13]. At 10 ppm, the degradation was even more severe and started at an earlier time [14]. While at 900 °C with 20 ppm $PH_3(g)$, the cell performance dropped immediately and sharply within 10 h [10].

Thermodynamically, $PH_3(g)$ shows the potential to react with Ni and forms mainly two compounds at low $PH_3(g)$ level:

$$2PH_3(g) + 5Ni \leftrightarrow Ni_5P_2 + 3H_2(g) \quad (5)$$

$$2PH_3(g) + 6Ni \leftrightarrow 2Ni_3P + 3H_2(g) \quad (6)$$

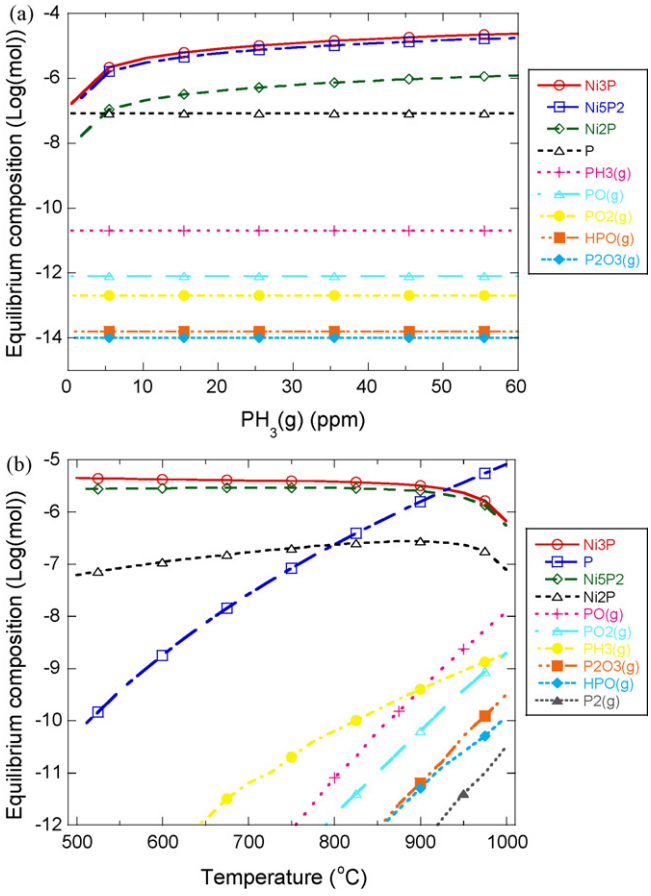

Fig. 6. Equilibrium compositions diagram of the phosphor containing species when Ni is in contact with P contaminated syngas. (a) $PH_3(g)$ concentration profile at 750 °C, (b) temperature profile at 10 ppm $PH_3(g)$.

The equilibrium constants at 750 °C for reaction (5) and (6) are 1.369×10^{21} and 4.791×10^{10}, respectively. Both reactions would shift toward the right direction with sub-ppm level $PH_3(g)$ and sub-atm level $H_2(g)$, and therefore nickel phosphides could be formed. Interestingly, direct XRD analysis after the cell was exposed to 20 ppm $PH_3(g)$ at 900 °C only found some phosphates [10]: $Ni_3(PO_4)_2$ and ZrP_2O_7, with the latter being found only at the open circuit condition. From Table 2, it is seen that $HPO_3(g)$ is the secondary populous P containing species under the SOFC operating conditions, so these phosphates may be formed through the reaction of $HPO_3(g)$ with Ni and ZrO_2 at the anode. Due to the lack of thermodynamic data for the phosphates, full equilibrium compositions of all the P containing species for this reaction system are not available.

Fig. 6 shows qualitative equilibrium compositions of the system if only phosphides are considered. From Fig. 6(a), the concentration profile at 750 °C, it is seen that over 99% of $PH_3(g)$ can react with Ni and forms mainly three types of phosphides, while the equilibrium amount of decomposed P and the partial pressure of $PH_3(g)$ remains constant at this concentration range (up to several hundred ppm). Under this operating environment: 750 °C and a few ppm of $PH_3(g)$, there is an incubation period for the poisoning effect of $PH_3(g)$ to be visible. Fig. 6(b) shows the temperature profile of the equilibrium composition at 10 ppm $PH_3(g)$. From 750 °C to 850 °C, the amount of phosphides decreases gradually, but the amount of P increases by an order of magnitude (reaching ppm level) and becomes comparable to other P species. Above 930 °C, P is the main specie, and other phosphides decompose quickly. As has been discussed in Part I, P can alloy with Ni, but the

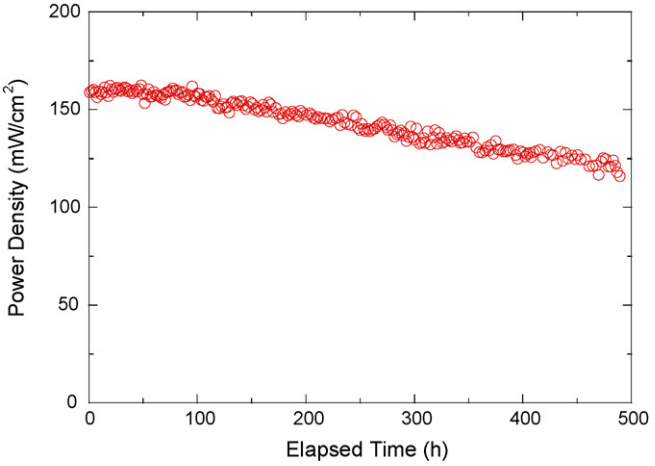

Fig. 7. Time evolution of the cell performance during the exposure to 2.5 ppm CH_3Cl(g) at 750 °C.

solubility of P is very low in Ni, and P tends to segregate from the bulk and forms a separate phase which could deteriorate the Ni catalyst interconnectivity for electron collection. Therefore, above 850 °C, even at ppm level, PH_3(g) could still be fatal.

Overall, it is concluded that both temperature and concentration level of phosphorous containing species affect the performance greatly, and high temperature operation (800 °C and above) seems to be very detrimental to the cell. At lower temperatures (e.g. 750 °C) and a few ppm (<5 ppm) below level, it takes over several hundred hours for the accumulative effects to be seen. But once the accumulated reaction products reach a certain value, the effect becomes significant. Therefore, the amount of PH_3(g) should be controlled to sub-ppm level by cleanup technologies.

3.6. Effect of ppm level CH_3Cl(g)

Methyl chloride was introduced by passing a carrier gas (H_2) through a permeation cell which releases CH_3Cl(g) at a rate of 511 ng min^{-1} (the K factor for CH_3Cl(g) is 0.484). The concentration level is approximately 2.5 ppm, and the time profile of the cell performance is shown in Fig. 7. Negligible performance variation is seen during the first 100 h test, but then a steady degradation occurred with a degradation rate of 0.1 mW/(cm^2 h). The power density dropped from 160 mW cm^{-2} to 120 mW cm^{-2} approximately within 400 h (6.25% per 100 h). The area specific resistance (ASR) increased appreciably from 1.05 Ω cm^2 to 1.75 Ω cm^2 approximately.

High temperature mass spectrometer shows that under the typical SOFC operating environment, CH_3Cl(g) is mainly dissociated into CH_4(g) and HCl(g), though the conversion is not complete. Cayan et al. [12] summarized the effect of chlorine species to the SOFC performance, including our accelerated test with 40 ppm CH_3Cl(g) and 40 ppm HCl(g). It is seen that except for our previous work, exposure to HCl(g) at 20 ppm and above all caused immediate and continuous degradation to the cell performance at 800 °C and above, and CH_3Cl(g) may be slightly more detrimental to the performance. However, the concentration levels are relatively too high to compare with the result in present work. Haga et al. [4] tested the effect of Cl_2(g) to the SOFCs at 800 °C with concentration levels of 5 ppm, 100 ppm and 1000 ppm. In their work, 5 ppm Cl_2(g) showed almost no degradation within 150 h's exposure, while 100 ppm and 1000 ppm Cl_2(g) resulted in 1.7% and 13% drop in power density per 100 h, respectively. They attributed the degradation to the formation of $NiCl_2$ compounds which is not likely according to our discussion in Part I, because $NiCl_2$ is not stable in reducing environment and will be reduced back to Ni and HCl(g) with the latter being the most stable chlorine specie in that environment. Therefore, the effect of chlorine species may be due to the continuous covering of the Ni catalyst surface by Cl.

After experiment characterization by SEM and EDX also did not find any chlorine species at the anode surface, and the structure and morphology of the anode remains almost intact. XRD analysis by Trembly [11] after the exposure to 160 ppm HCl(g) did not find any chlorine compounds, either. This further supports the conclusion that chlorine species are probably only bonded to the surface. If that is the case, the effect of HCl(g) should be reversible, as has been manifested that the ASR of the cell recovered back to the initial value after the removal of 160 ppm HCl(g). The continuous decline of the power density in our case may be due to some other effects not by chlorine species, this will be further verified in the work to continue (part III: synergetic effects).

3.7. Effect of ppm level H_2S(g)

Sulfur species are among the most widely studied contaminants to the SOFC performance. Cleanup technologies such as chemical and physical absorption systems are available to remove H_2S(g), but sub-ppm to ppm level of H_2S(g) may still be present in the coal-derived syngas fuel stream. Generally, immediate performance drop is seen after the addition of H_2S(g), even at sub-ppm level, followed by a slight degradation, and may establish a steady state in the long run [4,15–23]. The poisoning effect is worse at lower operating temperatures. A lot of controversies exist regarding the effect and mechanism of poisoning as has been discussed in Part I. Therefore, H_2S(g) at 1 ppm level is also tested at 750 °C in this work.

H_2S(g) was introduced by passing a carrier gas (H_2) through a permeation device which releases H_2S(g) at a rate of 205 ng min^{-1} (the K factor for H_2S(g) is 0.718). However, the Kitagawa precision detector tube for H_2S(g) (detection limit: 0.2–6 ppm) from Matheson Tri-gas measured only about 0.9–1 ppm level. From Fig. 8, it is seen that addition of H_2S(g) caused almost immediate performance drop (from 143.5 mW cm^{-2} to 138.5 mW cm^{-2} approximately, 3.5%) within the first 6 h (to be exact, the degradation started after about 45 min exposure), but then remained almost constant. Over the long-term, interestingly, the power density gradually recovered some portion of the initial loss to 141 mW cm^{-2} at the end of the test. The poisoning effect is fully reversible after the removal of the contaminant (not shown here, but will be demonstrated in the work to follow when the synergetic effects of contaminants are discussed in Part III), which indicates that the performance drop may be due to the adsorption of S at the Ni catalyst surface, blocking the active sites for the adsorption and dissociation of fuels, a mechanism similar to Cl species.

A stability diagram calculated thermochemically [4] shows that under the operating environment of the anode, formation of nickel sulfides is not likely unless the concentration level of the sulfur species reaches several thousand ppm. The equilibrium compositions for a system simulated to the syngas fed anode Ni–C–H–O–S are also calculated by HSC Chemistry®, as a function of the contaminant level at 750 °C, and as a function of the operating temperature at 100 ppm H_2S(g) level, see Fig. 9. From Fig. 9(a), it is seen that appreciable amount of nickel sulfide formation is not likely until above 3000 ppm H_2S(g) level at 750 °C. A vapor phase of nickel sulfide, NiS(g), forms at below 400 ppm level, but the amount is too negligible. Below 3000 ppm, S mainly exists in the form of H_2S(g), COS(g) and S, with H_2S(g) being the dominating specie. It is also noticed in Fig. 9(b) that about 1% of H_2S(g) decomposes to S (close to ppm level) even at concentrations below 50 ppm. The dissociated product could continuously deposit at the anode catalyst surface, and cause long-term performance degradation. If the deposited S diffuses into the Ni catalyst, then the poison effect may not be recov-

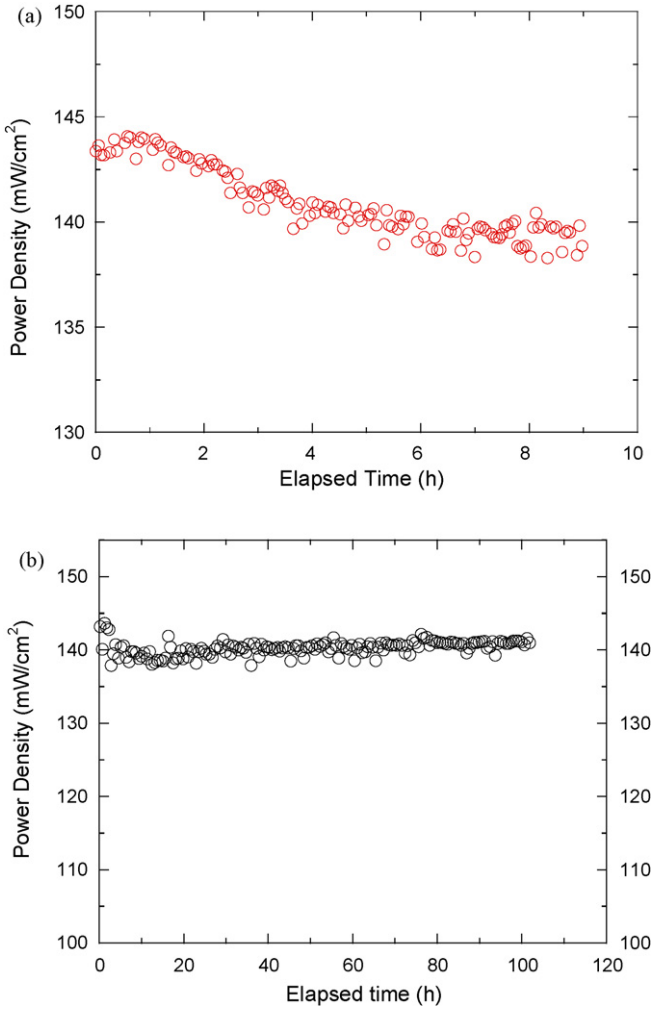

Fig. 8. Effect of 1 ppm $H_2S(g)$ to the cell performance at 750 °C. (a) First several hours, (b) overall time profile.

erable or require a long time to recover. This may be the main reason for the hovering controversies regarding the poisoning effect and mechanism of S poisoning. However, at the SOFC operating environment with a few ppm level and below, $H_2S(g)$ affects the cell performance most likely via the surface adsorption mechanism only.

Fig. 9(c) is the temperature profile of the equilibrium compositions of the system at 100 ppm level of $H_2S(g)$. Nickel sulfides are only stable below 480 °C approximately, and will decompose above that temperature. This critical temperature increases when the concentration of $H_2S(g)$ increases (550 °C approximately at 500 ppm and 460 °C approximately at 10 ppm). If the cell is cooled down in a contaminated fuel, various nickel sulfides would form during that cooling period, as has been manifested by in situ Raman microspectroscopy [22] that Ni_3S_4, β-NiS, and Ni_3S_2 were detected at the anode surface if the anode was cooled down in a fuel contaminated by $H_2S(g)$. While at high temperatures (500 °C and 570 °C) with the same $H_2S(g)$ level at 50 ppm, no sulfide was detected. Whether the cell was cooled down in a contaminant-free fuel or not may be the other reason contributing to the controversies over the poisoning mechanism of S.

Generally, it takes less than 10 h for the surface coverage of S to reach an equilibrium at ppm concentration level of $H_2S(g)$ (at 100 ml min^{-1} fuel flow rate, equivalent to 0.25 mol h^{-1}, and the surface atom density is assumed to be between 10^{15} and 10^{16} atoms cm^{-2}). While the accumulative effect of the deposited S may take up to 100 times longer to be appreciable as the equilibrium concentration of S is approximately two orders of magnitude lower than that of $H_2S(g)$. Therefore, if the cleanup technology could remove the amount of $H_2S(g)$ to a few ppm level and below, $H_2S(g)$ is not going to cause much harm to the cell performance except the initial performance loss.

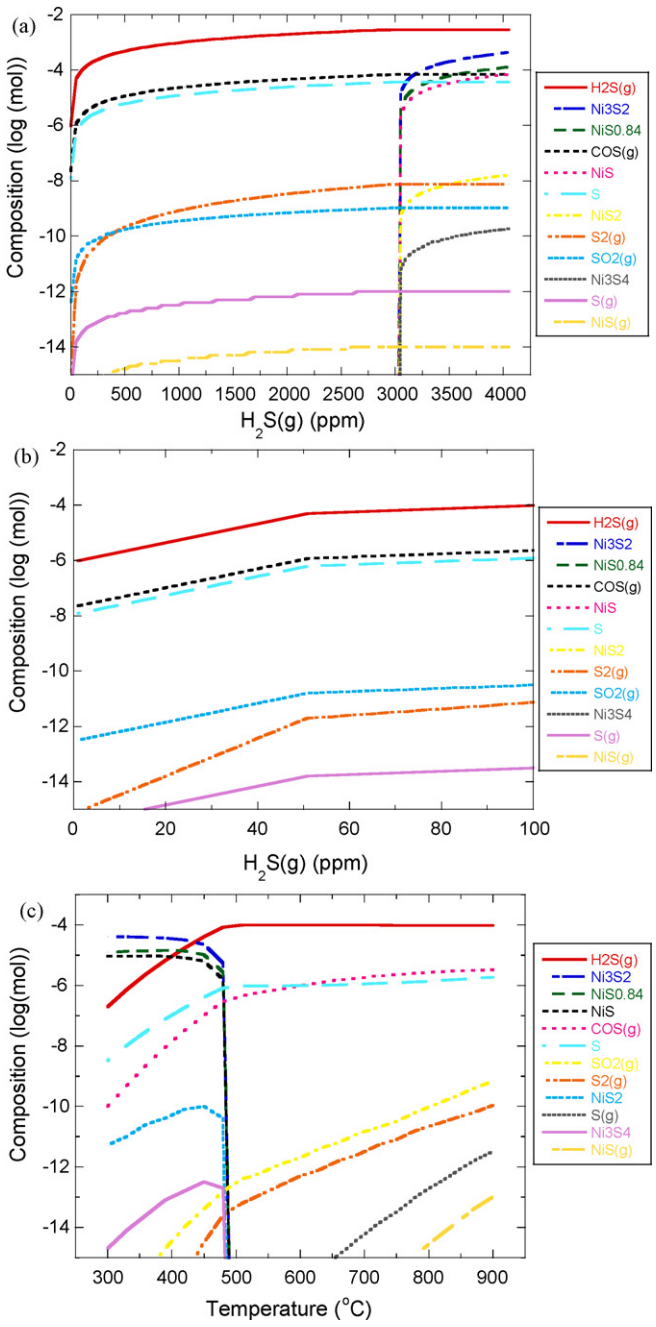

Fig. 9. Equilibrium composition diagram of the sulfur containing species when Ni catalyst is fed with the sulfur contaminated syngas. (a) $H_2S(g)$ concentration profile at 750 °C, (b) magnified diagram at low $H_2S(g)$ concentration level, and (c) temperature profile with 100 ppm $H_2S(g)$ contaminant.

4. Conclusions

The effects of various fuel contaminants at ppm and sub-ppm level to the performance of Ni-YSZ/YSZ/LSM SOFCs were studied, including Hg(g), $AsH_3(g)$, $PH_3(g)$, $CH_3Cl(g)$, and $H_2S(g)$. High temperature mass spectrometry analysis indicates that $PH_3(g)$ is only partially converted to $HPO_2(g)$ and $HPO_3(g)$, and $CH_3Cl(g)$ is also not

fully converted to CH_4(g) and HCl(g). Hg(g) at 180 ppb level did not cause any performance loss at 750 °C and 800 °C, but very slight decline occurred at 850 °C. The cell exposed to 0.5 ppm AsH_3(g) did not show any degradation during the 1000 h test at 750 °C, whereas at 1 ppm level, performance loss occurred after 700 h. Significant cell performance decline was observed after the cell was exposed to 0.5 ppm PH_3(g) at 750 °C for 350 h. Thermochemical calculations show that As and P can both form compounds with Ni, yet hydrolyzed P can also form phosphates with Ni and ZrO_2, inhibiting both the charge transfer step at the Ni catalyst surface and also the oxygen ion transport process through the YSZ electrolyte. Therefore, P is the most deleterious contaminant for the cell performance. CH_3Cl(g) at 2.5 ppm level resulted in the cell degradation after 100 h exposure, however, no Cl was detected at the anode by SEM and EDX after exposure. H_2S(g) at 1 ppm caused immediate performance loss, but then a slight increase was observed. The performance loss caused by Cl and S could both be recovered. Cl and S affect the anode most likely via the surface adsorption mechanism, blocking the reactive sites for the fuels. However, about 1% of H_2S(g) will also decompose to S which will deposit at the anode. The accumulative effect may become appreciable if the concentration level of H_2S(g) is above 100 ppm. At a few ppm and below, H_2S(g) may not cause much further degradation after the initial performance loss.

Acknowledgement

The authors would like to thank DOE for their financial supporting through the Contract No.: DE-FC26-05NT42627. The authors would also like to thank John. R. Albritton and Raghubir. P. Gupta from RTI International for their cooperative work on the test of AsH_3 and Hg.

References

[1] J.P. Trembly, R.S. Gemmen, D.J. Bayless, J. Power Sources 163 (2007) 986–996.
[2] Eastman Chemical Company, Project data on Eastman Chemical Company's Chemicals-From Coal Complex in Kingsport, TN, U.S. Department of Energy, 2003, 10–12.
[3] G.N. Krishnan, P. Jayaweera, J. Bao, J. Perez-Mariano, A. Sanjurjo, Journal of Power Sources, 2009, doi:10.1016/j.jpowsour.2009.04.034.
[4] K. Haga, S. Adachi, Y. Shiratori, K. Itoh, K. Sasaki, Solid State Ionics 179 (2008) 1427–1431.
[5] D.L. Hildenbrand, J. Chem. Phys. 48 (1968) 3657.
[6] D.L. Hildenbrand, J. Chem. Phys. 52 (1970) 5751.
[7] K.H. Lau, D.L. Hildenbrand, J. Chem. Phys. 86 (1987) 2949.
[8] L.V. Gurvich, I.V. Veyts, C.B. Alcock, Thermodynamic Properties of Individual Substances, vol.1, 4th edition, Hemisphere, New York, 1989.
[9] K.H. Lau, D.L. Hildenbrand, J. Chem. Phys. 100 (1994) 8373–8376.
[10] M. Zhi, X. Chen, H. Finklea, I. Celik, N.Q. Wu, J. Power Sources 183 (2008) 485–490.
[11] J.P. Trembly, R. Gemmen, D.J. Bayless, Proceedings of the 5th International Fuel Cell Science Engineering and Technology Conference, New York, NY, 2007.
[12] F.N. Cayan, M. Zhi, S.R. Pakalapati, I. Celik, N. Wu, R. Gemmen, J. Power Sources (2008), doi:10.1016/j.jpowsour.2008.06.058.
[13] O.A. Marina, L.R. Pederson, D.J. Edwards, C.W. Coyle, J. Templeton, M. Engelhard, Z. Zhu, Proceedings of the 8th Annual SECA Workshop, San Antonio, TX, 2007.
[14] O. Demircan, H. Finklea, J. Zondlo, C. Xu, The effect of PH3 impurity in coal syngas on SOFC performance, presented at Gordon Research Conference Electrochemistry Meeting, Ventura, CA, 2007.
[15] W. Feduska, A.O. Isenberg, J. Power Sources 10 (1983) 89–102.
[16] S.C. Singhal, R.J. Ruka, J.E. Bauerle, C.J. Spengler, Anode development for solid oxide fuel cells, Report No. DOE/MC/22046-2371, 1986.
[17] S.C. Singhal, K. Kendall, High Temperature Solid Oxide Fuel Cells: Fundamentals, Design and Applications, Elsevier, Oxford, England, 2003.
[18] M. Twigg, Catalyst Handbook, 2nd edition, Manson Publishing Ltd., London, England, 1996.
[19] Y. Matsuzaki, I. Yasuda, Solid State Ionics 132 (2000) 261–269.
[20] K. Sasaki, K. Susuki, A. Iyoshi, M. Uchimura, N. Imamura, H. Kusaba, Y. Teraoka, H. Fuchino, K. Tsujimoto, Y. Uchida, N. Jingo, J. Electrochem. Soc. 153 (2006) A2023–A2029.
[21] J.P. Trembly, A.I. Marquez, T.R. Ohrn, D.J. Bayless, J. Power Sources 158 (2006) 263–273.
[22] Z. Cheng, M. Liu, Solid State Ionics 178 (2007) 925–935.
[23] J.N. Kuhn, N. Lakshminarayanan, U.S. Ozkan, J. Mol. Catal. A: Chem. 282 (2008) 9–21.